Thermochemical and Kinetic Analyses on Oxidation of Isobutenyl Radical and 2-Hydroperoxymethyl-2-propenyl Radical

X. L. Zheng, H. Y. Sun,* and C. K. Law

Department of Mechanical and Aerospace Engineering, Princeton University, Princeton, New Jersey 08544

Received: April 8, 2005; In Final Form: July 6, 2005

In recognition of the importance of the isobutene oxidation reaction in the preignition chemistry associated with engine knock, the thermochemistry, chemical reaction pathways, and reaction kinetics of the isobutenyl radical oxidation at low to intermediate temperature range were computationally studied, focusing on both the first and the second O_2 addition to the isobutenyl radical. The geometries of reactants, important intermediates, transition states, and products in the isobutenyl radical oxidation system were optimized at the B3LYP/6-311G(d,p) and MP2(full)/6-31G(d) levels, and the thermochemical properties were determined on the basis of ab initio, density functional theory, and statistical mechanics. Enthalpies of formation for several important intermediates were calculated using isodesmic reactions at the DFT and the CBS-QB3 levels. The kinetic analysis of the first O_2 addition to the isobutenyl radical was performed using enthalpies at the CBS-QB3 and G3(MP2) levels. The reaction forms a chemically activated isobutenyl peroxy adduct which can be stabilized, dissociate back to reactants, cyclize to cyclic peroxide-alkyl radicals, and isomerize to the 2-hydroperoxymethyl-2-propenyl radical that further undergoes another O_2 addition. The reaction channels for isomerization and cyclization and further dissociation on this second O_2 addition were analyzed using enthalpies at the DFT level with energy corrections based on similar reaction channels for the first O_2 addition. The high-pressure limit rate constants for each reaction channel were determined as functions of temperature by the canonical transition state theory for further kinetic model development.

1. Introduction

It is of both practical and fundamental interest to study the chemical reaction pathways and kinetic mechanism of isobutene oxidation in the low to moderate temperature range. Practically, isobutene is a major oxidation intermediate of isooctane,[1] which, together with *n*-heptane, constitutes the reference fuels for the knock testing of spark-ignition engines. Furthermore, isobutene is also a major oxidation intermediate of methyl *tert*-butyl ether (MTBE) and ethyl *tert*-butyl ether (ETBE), which could be used as octane enhancers to replace lead additives to control engine knock.[2−5] Fundamentally, isobutene tends to react with active OH and H radicals through abstraction reactions to form the resonance-stabilized isobutenyl radical, which has low reactivity with oxygen in the combustion environment and exerts a high antiknock behavior in internal combustion engines. Therefore, studies of isobutenyl radical oxidation are warranted.

There have been several experimental studies on the oxidation of isobutene at various temperature and pressure ranges in the past decades.[6−11] These studies indicate that the primary reaction pathway for isobutene at moderate to high temperature and atmospheric pressure is the abstraction by reacting with active radicals to form the isobutenyl radical, which mostly decomposes to allene and the methyl radical.[6] At moderate temperature, the important reaction pathways include the addition of the OH radical to isobutene, the further addition of molecular oxygen, and the decomposition of the formed adduct to the products acetone, formaldehyde, and the hydroxyl radical.[8] At moderate temperature and high pressure, the formation of the HO_2 radical is favored so that the addition of HO_2 to both isobutene and the isobutenyl radical is the dominant consumption route for isobutene oxidation.[8] At low temperature, the H-abstraction reactions of isobutene are still dominant and provide an abundant amount of isobutenyl radical, but the combination of isobutenyl radicals and O_2 addition to the isobutenyl radical are also important reaction pathways.[11]

Chen and Bozzelli[12] recently analyzed the thermochemical and kinetic pathways of oxygen addition to the isobutenyl radical reactions by ab initio and density functional theory (DFT) calculations. They reported that, at low temperature, the concentration of isobutenyl peroxy radical is controlled by equilibrium instead of the formation rate from reactants. The barrier height for isomerization of the isobutenyl peroxy radical to 2-hydroperoxymethyl-2-propenyl radical is 20.70 kcal/mol, but further dissociation channels of the hydroperoxy isomer all involve high barriers. The nearly steady state between the isobutenyl peroxy radical and the 2-hydroperoxymethyl-2-propenyl radical makes the reaction paths of the 2-hydroperoxymethyl-2-propenyl radical with oxygen important in the reaction mechanism. In addition, this second O_2 addition is closely related to the two-stage ignition and the negative temperature coefficient (NTC) phenomena of the ignition delay time, such as those of *n*-pentane and 1-pentene.[13] Therefore, in the present study, we have investigated the thermochemical and kinetic pathways of the 2-hydroperoxymethyl-2-propenyl radical + O_2 system.

The kinetic reaction pathways analysis of the second O_2 addition system was performed at the density functional level. Since the first and second O_2 addition have some similar reaction pathways, we have also calculated several important reactions in the first O_2 addition to the isobutenyl radical system at the

* Author for correspondence. E-mail: hsun@princeton.edu.

10.1021/jp058116a CCC: $30.25
Published on Web 09/21/2005

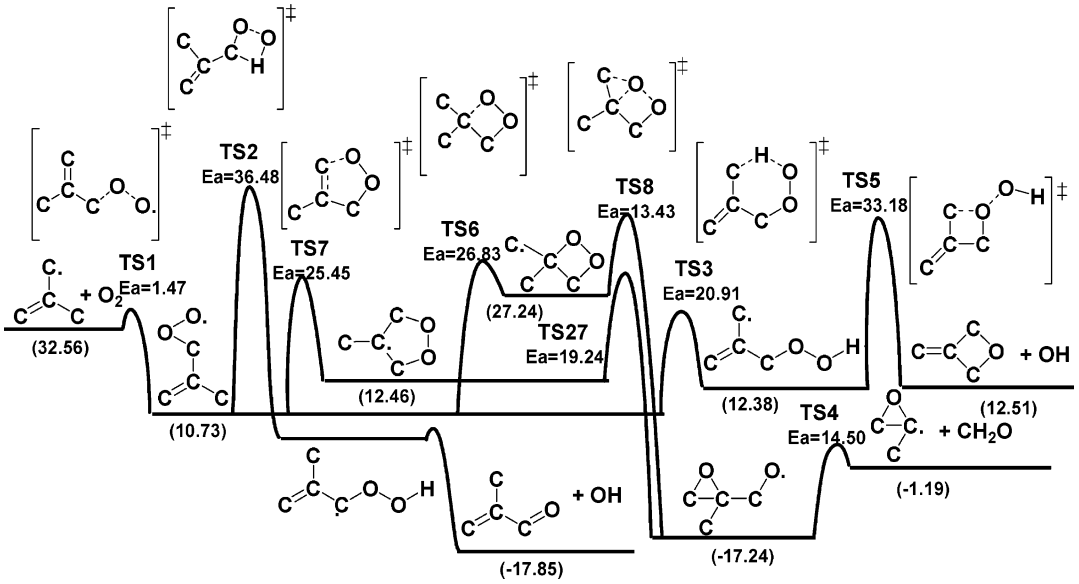

Figure 1. Potential energy diagram for the C═C(C•)C + O_2 reaction system. (Units in kcal/mol.)

higher CBS-QB3 and G3(MP2) levels and corrected the activation energies of similar reactions in the second O_2 addition by the energy differences between the high-level ab initio and DFT calculations for improved accuracy. The thermochemical properties for the species involved in the isobutene oxidation system were determined on the basis of ab initio, density functional theory, and statistical mechanics. The kinetic reaction pathways for the second O_2 addition to the isobutenyl radical were analyzed on the basis of the corrected DFT enthalpies, while the high-pressure limit rate constants were calculated by the canonical transition state theory.

2. Calculation Method

2.1. Computational Method. The total electronic energies for the first O_2 addition to the isobutenyl radical system were computed using the CBS-QB3[14] and G3(MP2)[15] methods. The CBS-QB3 method is a modified standard CBS-Q method and uses the B3LYP hybrid density functional structures and frequencies to achieve both enhanced reliability and improved accuracy, with little penalty in the computational cost. The G3-(MP2) method is a variation of the G3 theory[16] in which the basis set extensions are obtained at the second-order Møller−Plesset level. The G3(MP2) method is a significant improvement over the related G2(MP2) theory[17] and provides substantial savings in the computational time compared to both the G3 and G2(MP2) theories. Because of the relatively large molecular size, the total electronic energies for the second O_2 addition to the isobutenyl radical system were calculated at the B3LYP/6-311G(d,p) level, which is the same level as that of the CBS-QB3 method for geometry optimization and frequency calculation. All the computations were performed using the *Gaussian 03* program.[18]

2.2. Thermodynamic Properties. The entropies and heat capacities from vibrational, translational, and external rotational contributions were calculated using statistical mechanics based on the vibrational frequencies and structures obtained from the density functional study. Potential barriers for the internal rotations were calculated at the B3LYP/6-311G(d,p) level, and the hindered rotational contributions to $S°_{298}$ and $C_p(T)$ were calculated by using direct integration over energy levels of the internal rotational potentials.

The $\Delta H°_{f,298}$ values for several important intermediates were calculated using isodesmic reactions with total energies from DFT and ab initio calculations. The $\Delta H°_{f,298}$ of some intermediates were estimated by bond energies. The $\Delta H°_{f,298}$ of transition states were calculated by the $\Delta H°_{f,298}$ of the stable radical adducts plus the total energy differences between the radical adducts and the transition states.

2.3. Kinetic Analysis. Unimolecular dissociation and isomerization of the chemically activated and stabilized adducts resulting from addition reactions were analyzed by first constructing the potential energy diagrams for the reaction system. Then, the transition state structures and activation energies for the isomerization, β-scission, and dissociation reactions were determined by DFT and ab initio calculations. The enthalpies and entropies were further treated with the conventional transition state theory to calculate the Arrhenius preexponential factors and the activation energies that result in the high-pressure limit rate constants (k_∞) as functions of temperature. The high-pressure limit rate constants for several important isomerization reactions involving H transfer were further corrected to account for the tunneling effect.

3. Results and Discussion

3.1. Geometries of Reactants, Intermediates, Transition States, and Products. The geometries of reactants, intermediates, transition states, and products were optimized at the B3LYP/6-311G(d,p) and MP2(full)/6-31G(d) levels for species in the first O_2 addition to the isobutenyl radical system (Figure 1) and at the B3LYP/6-311G(d,p) level for species in the second O_2 addition system (Figure 2a,b). The transition state (TS) structures were preoptimized at the PM3 level and then followed by optimization and frequency calculation at the DFT level. All the transition state structures were identified by having only one imaginary frequency with motion along the reaction coordinate. The optimized structural parameters for 50 species are listed in Table S-1 of the Supporting Information, their corresponding unscaled vibrational frequencies and moments of inertia are listed in Table S-2, and the names of the important species calculated in this study are defined in Table S-3.

Chen and Bozzelli[12] calculated the structures of most species involved in the first O_2 addition to the isobutenyl radical at the B3LYP level, but with a smaller basis set: 6-31G(d). The structures optimized in the first O_2 addition system at the B3LYP/6-311G(d,p) level are very close to their published

values. The optimized structures investigated in this study are discussed as follows.

The optimized geometries for stable molecules between the B3LYP/6-311G(d,p) and MP2(full)/6-31(d) levels are in good agreement; differences of bond lengths are within 0.024 Å, bond angles are within 1.9°, and dihedral angles are within 9.0°. However, the active transition bond lengths in the optimized transition state structures show larger differences between the DFT and MP2 levels. The transition states of important reactions in this oxidation system are identified as follows, and the geometric parameters are based on the calculation at the B3LYP/6-311G(d,p) level.

Alkyl Peroxy Radical Isomerization. These reactions are endothermic, with intramolecular H-atom transfer from the $-CH_3$ (TS3), $-CH_2$ (TS9), or $=CH_2$ (TS11) group to the peroxy oxygen radical site. These isomerization reactions are through six-membered-ring transition states. The cleaving C—H bond is stretched from 1.09 Å to 1.34−1.48 Å, and the O—H bond formed is about 1.11−1.24 Å. In TS11, the C_{sp2}—H bond is stretched to 1.48 Å, which is 0.1 Å longer than the stretched C_{sp3}—H bond length, since the ring strain is increased by the existence of a C=C bond in this six-membered-ring transition state.

Oxetane and Oxetene Formation. In this reaction type, the carbon radical in the $-CH_2^\bullet$ or $=CH^\bullet$ group attacks the peroxy oxygen to form a four-membered-ring transition state, and the weak RO—OH bond breaks (TS5, TS12, TS14). The forming C—O bond length is about 1.96−1.99 Å, and the cleaving O—O bond is stretched from 1.48 Å to 1.67−1.75 Å. This reaction contributes to the OH radical formation.

H Elimination from the R—$CH_2O^\bullet$ Group. In these reactions, the H atom dissociates from the $-CH_2O^\bullet$ group forming the R—CHO group (TS13, TS16). The cleaving C—H bond is stretched from 1.09 Å to about 1.81−1.84 Å, and the C=O bond formed is shortened from 1.43 Å to 1.22 Å. This reaction contributes to the H-radical formation.

OH Elimination from the Alkyl Peroxy Group. In this reaction type, the peroxy oxygen radical attacks the H atom in the adjacent carbon via a four-membered-ring transition state (TS2, TS10). The reaction path passes through a transient intermediate R—C$^\bullet$OOH, for which the carbon radical forms a π bond with oxygen, and the weak O—OH bond breaks.[19] The C—O and O—H bond lengths are 1.39 and 1.35 Å, respectively. The transient intermediate R—C$^\bullet$OOH leads to the products R—CH(=O) + OH.

β-Scission of Alkyl Radicals. These reactions involve the cleavage of the C—C bond near the radical site and the formation of formaldehyde or the formyl radical (TS4, TS15, TS19). The C—C bond is stretched from 1.54 Å to 2.21−2.25 Å, and the C—O bond is shortened from 1.36 Å to 1.23 Å.

3.2. Internal Rotation Analysis. The potential barriers for internal rotations of all stable species were calculated at the B3LYP/6-311G(d,p) level. The potential energy was determined as a function of dihedral angles by varying the torsion angle in 15° intervals and allowing the remaining molecular structures to be optimized. The internal rotation barriers were determined as the total energy differences between each conformation and the most stable conformer. This internal rotation analysis can locate the most stable conformer of the species and therefore ensures the accuracy of the optimized geometries.

Some calculated rotation potentials are demonstrated in Figures S1−S3 of the Supporing Information for the three most frequently encountered C—C, C—O, and O—O bonds. The C—C bond rotation potential (Figure S1) is symmetric and exhibits threefold barriers corresponding to the rotation of the $C—CH_3$ bond. The C—OOH rotations for C=C(C$^\bullet$)COOH, C=C(COO$^\bullet$)COOH, and C$^\bullet$C(CHO)COOH (Figure S2) have a typically higher barrier of 6.1−7.6 kcal/mol. However, the barrier height of the C—OO$^\bullet$ rotation in C=C(C)COO$^\bullet$ is only about 3.0 kcal/mol due to the lack of interaction between the peroxy H atom with its neighboring groups. The calculated barrier heights of the O—O bond for C=C(C$^\bullet$)COOH, C$^\bullet$=C(CHO)COOH, and Cy(C$^\bullet$COOC)COOH are about 5.8−6.8 kcal/mol (Figure S3), which is in close agreement with the published barrier height of O—O bond rotation.[20,21] All these potential barrier curves were further used to calculate the contributions from internal rotors to entropy and heat capacities, which will be discussed in detail in the next section.

3.3. Thermodynamic Properties. *Entropies $S°_{298}$ and Heat Capacities C_p(300 K) to C_p(1500 K).* On the basis of statistical mechanics, the vibrational frequencies and moments of inertia from the optimized B3LYP/6-311G(d,p) structures were used to calculate the contributions to entropies and heat capacities from vibration, translation, and external rotation (TVR) by the SMCPS[22] program. The contributions to $S°_{298}$ and $C_p(T)$ from the torsion frequencies were not treated as vibrations, but rather as internal rotations (IR). These contributions were determined by solving the Schrödinger equation with free rotor wave functions, and the partition coefficients were obtained by direct integration over the energy levels of intramolecular rotational potential curves, such as Figures S1−S3, which were represented by a truncated Fourier series expansion. The contributions to $S°_{298}$ and $C_p(T)$ values from the hindered internal rotation along C—C, C—O, and O—O bonds in several species are listed in Table S4 of the Supporting Information as examples. The rotation potentials for the transition state structures were not calculated; their contributions to $S°_{298}$ and $C_p(T)$ were assumed to be the same as those of their corresponding reactants or products.

Enthalpies of Formation. The enthalpies of formation for species in the isobutenyl radical oxidation system were calculated by three methods. First, the enthalpies of formation for the three important species, namely C=C(C)COO$^\bullet$, C=C(COO$^\bullet$)COOH, and C=C(CHO)COOH, were calculated using isodesmic reactions as listed in Table 1, together with the calculated heats of reaction and enthalpies of formation. In each isodesmic reaction, density functional and ab initio calculations with zero-point vibrational energy (ZPVE) and thermal corrections were performed for all four compounds, and the enthalpy of reaction $\Delta H_{rxn,298}$ was determined as the total energy difference between products and reactants. Since the $\Delta H°_{f,298}$ values of the three reference species are available from the literature, the enthalpy of formation of the target species could be calculated through an algebraic equation.

As shown in Table 1, the $\Delta H°_{f,298}$ values of C=C(C)COO$^\bullet$, calculated using isodesmic reactions at the DFT and CBS-QB3 levels, differ by only 0.4 kcal/mol, indicating that computational errors were canceled out to a great extent for different species. The average value of $\Delta H°_{f,298}$ at the CBS-QB3 level is recommended here. For C=C(COO$^\bullet$)COOH and C=C(CHO)COOH, the isodesmic reaction calculations were performed only at the DFT level because of their larger molecular sizes. In addition, the $\Delta H°_{f,298}$ values of C=C(C)COOH and C=C(COOH)$_2$, the parents of the C=C(C)COO$^\bullet$ and C=C(COO$^\bullet$)COOH radicals, were also calculated using isodesmic reactions, which are needed to calculate the $\Delta H°_{f,298}$ values of their corresponding radicals.

TABLE 1: Calculated $\Delta H^\circ_{f,298}$ (kcal/mol) by Isodesmic Reactions[a]

	B3LYP/6-311G(d,p)		CBS-QB3	
	ΔH°_{rxn}	$\Delta H^\circ_{f,298}$	ΔH°_{rxn}	$\Delta H^\circ_{f,298}$
C═C(C)COOH + C═CC + CH_3OH → C═C(C)C + C═CCOH + CH_3OOH	−1.58	−21.27	0.04	−22.89
average of $\Delta H^\circ_{f,298}$ for C═C(C)COOH		−21.27		−22.89
C═C(C)COO• + CH_3OOH → C═C(C)COOH + CH_3OO•	−0.06	10.22	−0.33	10.49
C═C(C)COO• + C_2H_5OOH → C═C(C)COOH + C_2H_5OO•	−0.43	10.44	−0.96	10.97
average of $\Delta H^\circ_{f,298}$ for C═C(C)COO•		10.33		10.73
C═C(COOH)$_2$ + 2CH_4 → C_2C═C + 2CH_3OOH	10.62	−40.44		
C═C(COOH)$_2$ + CH_4 + C_2H_6 → C_2C═C + CH_3OOH + C_2H_5OOH	5.27	−41.74		
average of $\Delta H^\circ_{f,298}$ for C═C(COOH)$_2$		−41.09		
C═C(COO•)COOH + CH_3OOH → C═C(COOH)$_2$ + CH_3OO•	−2.34	−5.70		
C═C(COO•)COOH + C_2H_5OOH → C═C(COOH)$_2$ + C_2H_5OO•	−2.71	−5.48		
average of $\Delta H^\circ_{f,298}$ for C═C(COO•)COOH		−5.59		
C═C(CHO)COOH + 2CH_4 → C═C(C)C + CH_3OOH + CH_2O	14.80	−39.66		
C═C(CHO)COOH + CH_4 + C_2H_6 → C═C(C)C + CH_3OOH + CH_3CHO	3.07	−39.56		
C═C(CHO)COOH + CH_4 + C_2H_6 → C═C(C)C + C_2H_5OOH + CH_2O	9.44	−40.95		
average of $\Delta H^\circ_{f,298}$ for C═C(CHO)COOH		−40.06		

[a] Literature data used in isodesmic reaction: $\Delta H^\circ_{f,298}$ of (CH_3OOH) = −30.9 (ref 23); (C_2H_5OOH) = −39.7 (ref 24); (CH_3OO•) = 2.15 (ref 25); (C_2H_5OO•) = −6.8 (ref 23); (C═CCOH) = −31.52 (ref 26); (C═C(C)C) = −3.8 (ref 27); (C═CC) = 4.71 (ref 26); (CH_3OH) = −48.08 (ref 28); (CH_4) = −17.89 (ref 28); (C_2H_6) = −20.04 (ref 28); (CH_2O) = −25.94 (ref 26); (CH_3CHO) = −39.72 (ref 26); in kcal/mol.

Second, the enthalpies of formation for C•═C(COOH)$_2$ and C•═C(CHO)COOH were estimated by the bond energies. On the basis of the above isodesmic reactions, the $\Delta H^\circ_{f,298}$ values for the corresponding stable species C═C(COOH)$_2$ and C═C(CHO)COOH were determined to be −41.09 and −40.06 kcal/mol, respectively. The H—C═R bond energy for these two species was taken as 110 kcal/mol, the same as that of ethene. Consequently, the estimated $\Delta H^\circ_{f,298}$ values of C•═C(COOH)$_2$ and C•═C(CHO)COOH are 16.81 and 17.84 kcal/mol, respectively.

Finally, the enthalpies of formation for the transition states and other species were calculated directly by adding the calculated total energy differences between the adducts and the reactants to the $\Delta H^\circ_{f,298}$ values of the stabilized adducts. The calculated total energy differences were based on the CBS-QB3 calculation for species in the first O_2 addition system and on either the DFT or the corrected CBS-QB3 calculation for species in the second O_2 addition system.

The enthalpies of formation, entropies, and heat capacities are summarized in Table 2 for all important reactants, intermediates, transition states, and products in the isobutenyl radical oxidation system. These thermal data constitute an essential component for the isobutene oxidation mechanism.

3.4. Analysis of Chemical Activation Reactions. *C═C(C•)C + O_2.* The first O_2 addition to the isobutenyl radical reaction system was theoretically analyzed by Chen and Bozzelli,[12] and the thermochemical and kinetic pathways of oxygen addition to the isobutenyl radical reactions were reported at the CBS-q//MP2(full)/6-31G(d) level. In this study, we calculated several important channels in the first O_2 addition system at the higher CBS-QB3 and G3(MP2) levels in order to evaluate/calculate the activation energies of similar reactions in the second O_2 addition system.

A number of reaction channels in the C═C(C•)C + O_2 system calculated in this study are shown in Figure 1. The isobutenyl radical reacts with O_2 and forms a chemically activated C═C(C)COO•* adduct. The major reaction channels of the C═C(C)COO•* adduct include dissociation back to reactants, stabilization to C═C(C)COO•, and isomerization through H shift to the peroxy radical site to form the isomers C═C(C•)COOH (via TS3, E_a = 20.91 kcal/mol) and C═C(C)C•OOH (via TS2, E_a = 36.48 kcal/mol), which dissociates rapidly to C═C(C)-CHO + OH. The adduct C═C(C)COO•* can also cyclize to form a dioxetane (via TS6, E_a = 26.83 kcal/mol) or dioxolan (via TS7, E_a = 25.45 kcal/mol) radical. For the C_2•CyCOOC and CCyC•COOC intermediates, the carbon radical can attack the O atom (via TS8, E_a = 13.43 kcal/mol, and TS27, E_a = 19.24 kcal/mol) to form a three-membered-ring structure with the O—O bond broken simultaneously. The CCy(COC)CO• radical formed undergoes further β-scission (via TS4, E_a = 14.50 kcal/mol) to CCy(C•OC) and formaldehyde.

The total energy differences between TSs and reactants, intermediates, and products of the reactions involved in the first O_2 addition to the isobutenyl radical system were calculated at the DFT, CBS-QB3, and G3(MP2) levels and are listed in Table 3a. Overall, the activation energies calculated at these three levels show good agreement. The activation energies at the CBS-QB3 level are generally lower than those of the G3(MP2) level, and the difference is up to 6 kcal/mol. In the present study, the activation energies of reactions in this system were taken from the CBS-QB3 level calculation.

Table 3a also lists the activation energies calculated at the CBS-q level by Chen and Bozzelli.[12] These calculated activation energies agree with values at the CBS-QB3 level in general, but a few reactions, including TS1, TS5, and TS8, show larger discrepancies.

For the reaction C═C(C•)C + O_2 → C═C(C)COO• (via TS1), the activation energies calculated at three levels all assume negative values. Chen and Bozzelli[12] calculated this activation energy at the B3LYP/6-311+G(d,p)//B3LYP/6-31 g(d) and G3(MP2) levels and also obtained small negative values. They suggested the reaction barrier to be 1.47 kcal/mol[12] based on calculations at the CBS-q//MP2(full)/6-31g(d) level, and previous experiments[29−31] which indicated that the similar reaction of allyl radical + O_2 → allyl peroxy radical has no significant barrier. Therefore, we adopt their recommended E_a value of 1.47 kcal/mol.

The isomer C═C(C•)COOH formed by H-shift isomerization can further dissociate (via TS5) to OH + C═CyCCOC. The activation energies for TS5 at the G3(MP2)[32] and CBS-q[12] levels are both around 40 kcal/mol, which is about 7 kcal/mol higher than the CBS-QB3 value, but the CBS-QB3 value is closer to that at the DFT level (30.62 kcal/mol). The activation energy of similar hydroperoxy-neopentyl radical dissociation reaction (C_3•CCOOH → C_2CyCCOC + OH) was reported as 15.50 kcal/mol at the CBS-Q level.[19] For the 2-hydroperoxymethyl-2-

TABLE 2: Ideal Gas-Phase Thermodynamics Properties for Species

	$\Delta H°_{f,298}$ (kcal/mol)	$S°_{298}$ (kcal/mol)	C_p300 (cal/mol−K)	C_p400	C_p500	C_p600	C_p800	C_p1000	C_p1500
			1st O_2 Addition						
C═C(C•)C	32.56[a]	71.46	19.52	24.90	29.48	33.28	39.16	43.55	50.52
C═C(C)COO•	10.73	90.20	26.28	31.77	36.61	40.68	46.94	51.52	58.62
C═C(C•)COOH	12.38	89.23	31.49	36.18	40.21	43.61	48.91	52.87	59.22
C═CyCCOC	3.62	68.98	18.98	24.80	29.94	34.20	40.66	45.27	52.20
C═C(C)C═O	−26.74	75.43	21.44	26.64	31.31	35.22	41.12	45.26	51.23
C_2•CyCOOC	27.24	82.18	26.89	33.36	38.73	43.05	59.52	54.19	61.39
CCyC•COOC	12.46	81.05	23.23	29.86	35.82	40.82	48.42	53.83	61.87
CCy(CCO)CO•	−17.24	83.26	25.77	31.87	37.26	41.74	48.54	53.40	60.71
CCyC•CO	24.75	68.98	18.98	24.80	29.94	34.20	40.66	45.27	52.20
TS0	88.80	77.93	23.33	27.82	31.57	34.68	39.63	43.48	49.88
TS1	34.03[a]	85.10	26.97	32.63	37.52	41.62	47.97	52.67	60.04
TS2	47.21	82.74	25.93	32.08	37.40	41.81	48.54	53.36	60.64
TS3	31.64	76.84	24.25	31.33	37.29	42.12	49.26	54.23	61.61
TS4	−2.74	85.91	26.01	31.49	46.48	40.76	47.51	52.47	60.08
TS5	45.56	83.15	27.23	33.50	38.72	42.92	49.22	53.78	60.96
TS6	37.56	79.01	25.24	31.57	36.96	41.37	48.02	52.82	60.22
TS7	36.18	78.95	22.89	29.40	35.10	39.82	46.98	52.11	59.89
TS8	40.67	78.39	25.44	31.86	37.26	41.64	48.23	52.98	60.29
			2nd O_2 Addition						
C═C(COO•)COOH	−5.59	101.86	38.24	44.67	49.69	53.61	59.30	63.32	69.53
C═C(CHO)COOH	−40.06	96.57	29.36	34.58	39.21	43.09	49.00	53.24	59.70
C•═C(COOH)$_2$	16.81	107.86	40.30	46.14	50.51	53.80	58.49	61.87	67.32
C•═C(CO•)COOH	46.72	92.88	33.67	40.02	45.11	48.98	54.22	57.50	61.83
Cy(C═COC)COOH	−13.79	87.72	27.52	33.93	39.43	43.88	50.39	54.90	61.57
C•═C(CHO)COOH	17.84	97.55	29.70	34.22	38.16	41.42	46.38	49.91	55.24
Cy(C═COC)CHO	−19.52	74.12	20.28	25.36	29.86	33.57	39.11	42.94	48.48
C═C(C•)CHO	−4.63	73.55	21.17	26.12	30.22	33.55	38.60	42.24	47.83
C═C(CO•)CHO	−10.46	83.94	23.75	28.92	33.34	37.00	42.50	46.39	52.12
C═C(CHO)$_2$	−45.62	76.24	22.30	26.85	30.85	34.23	39.43	43.12	48.56
Cy(C•COOC)COOH	−1.95	101.45	31.87	38.96	45.12	50.13	57.55	62.70	70.32
C•Cy(COOC)COOH	13.40	97.11	36.55	44.12	50.06	54.51	60.57	64.64	70.82
CO•Cy(COC)COOH	−29.80	96.48	38.15	45.82	51.42	55.34	60.52	64.11	69.89
Cy(C•OC)COOH	9.46	84.08	27.36	32.71	36.62	39.53	43.58	46.36	50.61
C═C═C	46.72	57.95	13.88	16.90	19.50	21.66	25.05	27.62	31.74
C═C(COOH)$_2$	−41.09	94.31	38.36	49.49	58.09	63.68	69.14	71.60	75.33
CyC═COC−CO•	16.72	78.56	22.52	28.24	33.21	37.27	43.30	47.49	53.60
C•C(═O)COOH	−27.79	84.16	29.98	34.91	38.55	41.32	45.20	47.81	51.63
O═CyCCOC	−44.04	70.45	17.23	21.90	25.96	29.31	34.32	37.82	42.95
TS9	14.49	88.80	32.53	40.78	47.56	52.88	60.38	65.41	72.67
TS10	32.39	93.80	35.36	42.64	48.54	53.17	59.82	64.38	71.15
TS11	25.41	95.49	37.28	44.41	49.82	53.96	59.85	63.89	69.96
TS12	37.23	100.08	36.12	42.98	48.55	52.90	59.14	63.51	70.30
TS13	71.70	92.01	32.44	39.09	44.45	48.59	54.32	57.99	62.91
TS14	36.17	88.36	28.62	33.98	38.49	42.14	47.60	51.46	57.32
TS15	41.81	80.65	22.98	26.98	30.35	33.16	37.59	40.93	46.19
TS16	10.22	85.08	25.25	30.08	34.14	37.49	42.50	46.00	51.08
TS17	21.49	96.61	32.12	39.51	45.59	50.37	57.23	61.95	68.99
TS18	19.35	94.87	34.82	42.17	48.10	52.65	58.94	63.19	69.61
TS19	−14.34	101.47	37.24	44.51	49.94	53.83	59.16	62.98	69.18
TS20	−1.83	82.88	25.46	30.53	34.66	37.95	42.83	46.32	51.72
TS21	39.21	76.51	22.04	27.83	32.70	36.60	42.33	46.28	52.04
TS22	13.85	104.33	34.71	41.68	47.54	52.31	59.46	64.56	72.36

[a] Data was taken from ref 12.

propenyl radical, an additional ca. 14 kcal/mol increase in the barrier height is required for the loss of resonance stabilization to form TS5. Consequently, the activation energy is around 15.5 + 14 = 29.5 kcal/mol, which is close to our DFT and CBS-QB3 calculations. Therefore, we recommend the activation energy for TS5 to be 33.18 kcal/mol. The lower activation energy as compared to the previous value from the CBS-q level[12] increases the importance of this reaction channel for the OH radical formation.

The C_2•CyCOOC radical is formed via intramolecular addition of the terminal oxygen radical to the C═C π bond (TS6), which has a relatively high barrier height of 26.83 kcal/mol due to the nearly complete loss of the C═C π-bond energy. The carbon radical in the C_2•CyCOOC radical can attack the O atom (via TS8) to form a three-membered-ring structure, and the O−O bond in the original four-membered-ring breaks simultaneously. The calculated E_a values for TS8 are 11.21, 13.43, and 11.08[33] kcal/mol at the DFT, CBS-QB3, and G3(MP2) levels, ca. 6 kcal/mol lower than the reported value.[12] Here, we take the E_a values to be 13.43 kcal/mol at the CBS-QB3 level.

The above kinetic analyses confirm again that the isobutenyl radical has relatively low reactivity toward oxygen. The calculated well depth for C═C(C•)C + O_2 → C═C(C)COO• is only 20.91 kcal/mol, which is about 14 kcal/mol lower than those of the alkyl radical + O_2 systems. The shallow well depth, a consequence of losing the resonance stabilization,[12] causes the peroxy adduct C═C(C)COO• to dissociate back to reactants rapidly. Nevertheless, the isomerization reaction forming C═

TABLE 3: Total Energy (at 298 K) Differences between TSs and Reactants, Intermediates, and Products (kcal/mol)

(a) First O_2 Addition to the Isobutenyl Radical System

reactions	B3LYP	CBS-QB3	G3MP2	CBS-q[a]
C═C(C•)C → TS0	53.83	56.24	56.39	N/A
C═C(C•)C + O_2 → TS1	−0.91	−6.07	−6.00	1.47
C═C(C)COO• → TS1	14.21	14.84	15.58	22.97
C═C(C)COO• → TS2	38.62	36.48	39.80	39.57
C═C(C)C═O + OH → TS2	65.06	65.06	70.23	69.48
C═C(C)COO• → TS3	21.96	20.91	24.74	20.70
C═C(C•)COOH → TS3	16.31	19.27	21.89	20.57
CCy(CCO)CO• → TS4	13.55	14.50	14.72	N/A
CCy(C•CO) + CH_2O → TS4	0.07	1.56	1.01	N/A
C═C(C•)COOH → TS5	30.62	33.18	39.33	41.27
C═CyCCOC + OH → TS5	30.00	33.05	41.55	41.94
C═C(C)COO• → TS6	30.09	26.83	29.56	29.85
C2•CyCOOC → TS6	6.57	10.32	12.18	11.18
C═C(C)COO• → TS7	27.51	25.45	28.54	28.17
CCyC•COOC → TS7	21.87	23.72	24.48	26.57
C_2•CyCOOC → TS8	11.21	13.43	11.08	19.67
CCy(CCO)CO• → TS8	58.69	57.91	58.84	63.60

(b) Second O_2 Addition System

reactions	B3LYP
C═C(COO•)COOH → TS9	21.13
C═C(CHO)COOH + OH → TS9	43.07
C═C(COO•)COOH → TS10	40.12
C═C(CHO)COOH + OH → TS10	62.06
C═C(COO•)COOH → TS11	31.00
C•═C$(COOH)_2$ → TS11	3.24
C•═C$(COOH)_2$ → TS12	20.42
Cy(C═COC)COOH + OH → TS12	42.13
C•═C$(COOH)_2$ → C•═C(CO•)COOH + OH	38.80
C•═C(CO•)COOH → TS13	24.97
C•═C(CHO)COOH + H → TS13	5.06
C•═C(CHO)COOH → TS14	18.33
Cy(C═COC)CHO + OH → TS14	46.80
C═C(CHO)COOH → C═C(C•)CHO + HO_2	45.12
C═C(C•)CHO → TS15	46.43
C═C═C + HCO → TS15	7.59
C═C(CHO)COOH → C═C(CO•)CHO + OH	38.49
C═C(CO•)CHO → TS16	20.68
C═C$(CHO)_2$ + H → TS16	3.75
C═C(COO•)COOH → TS17	29.13
Cy(C•COOC)COOH → TS17	23.43
C═C(COO•)COOH → TS18	28.20
C•Cy(COOC)COOH → TS18	5.95
CO•Cy(COC)COOH → TS19	15.45
Cy(C•OC)COOH + CH_2O → TS19	2.14
C•C(═O)COOH → TS20	25.96
O═CyCCOC + OH → TS20	33.32
Cy(C═COC)COOH → Cy(C═COC)CO• + OH	39.40
Cy(C═COC)CO• → TS21	22.49
Cy(C═COC)CHO + H → TS21	9.94
C═C(C•)COOH + O_2 → TS22	1.47
C═C(COO•)COOH → TS22	19.44

[a] Data was taken from ref 12.

C(C•)COOH via TS3 has the same reaction barrier of 20.91 kcal/mol as the well depth, so the other competing channel for the C═C(C)COO• adduct is to isomerize to C═C(C•)COOH.

In addition, the further dissociations of the isomer C═C(C•)-COOH have significantly high barriers;[12] the lowest barrier for the dissociation channel to OH + C═CyCCOC was calculated to be 33.18 kcal/mol in this study. As indicated by Chen and Bozzelli,[12] the major reaction flux of C═C(C•)COOH is therefore either to isomerize back to C═C(C)COO• or to further react with O_2.

C═C(C•)COOH + O_2. The above analysis of the first O_2 addition has revealed that one dominant reaction for the adduct C═C(C)COO•* is isomerization to C═C(C•)COOH: the 2-hydroperoxymethyl-2-propenyl radical. C═C(C•)COOH can undergo another O_2 addition reaction, for which the potential energy diagrams are calculated at the B3LYP/6-311G(d,p) level and shown in Figure 2.

For the reaction C═C(C•)COOH + O_2 → C═C(COO•)COOH (via TS22), we were not able to locate the structure of TS22 at the DFT level. Instead, the optimized structures of TS22 were identified at the PM3 level and are listed in Table S-1 of the Supporting Information. The PM3 structure was then used for the total electronic energy calculation at the B3LYP/6-311G-(d,p) level, which leads to an unreasonably high activation energy of 5.03 kcal/mol. Since this second O_2 addition reaction is similar to the first O_2 addition reaction C═C(C•)C + O_2 → C═C(C)COO• (via TS1), we choose the activation energy of TS22 to be 1.47 kcal/mol, which is the same as that of TS1.

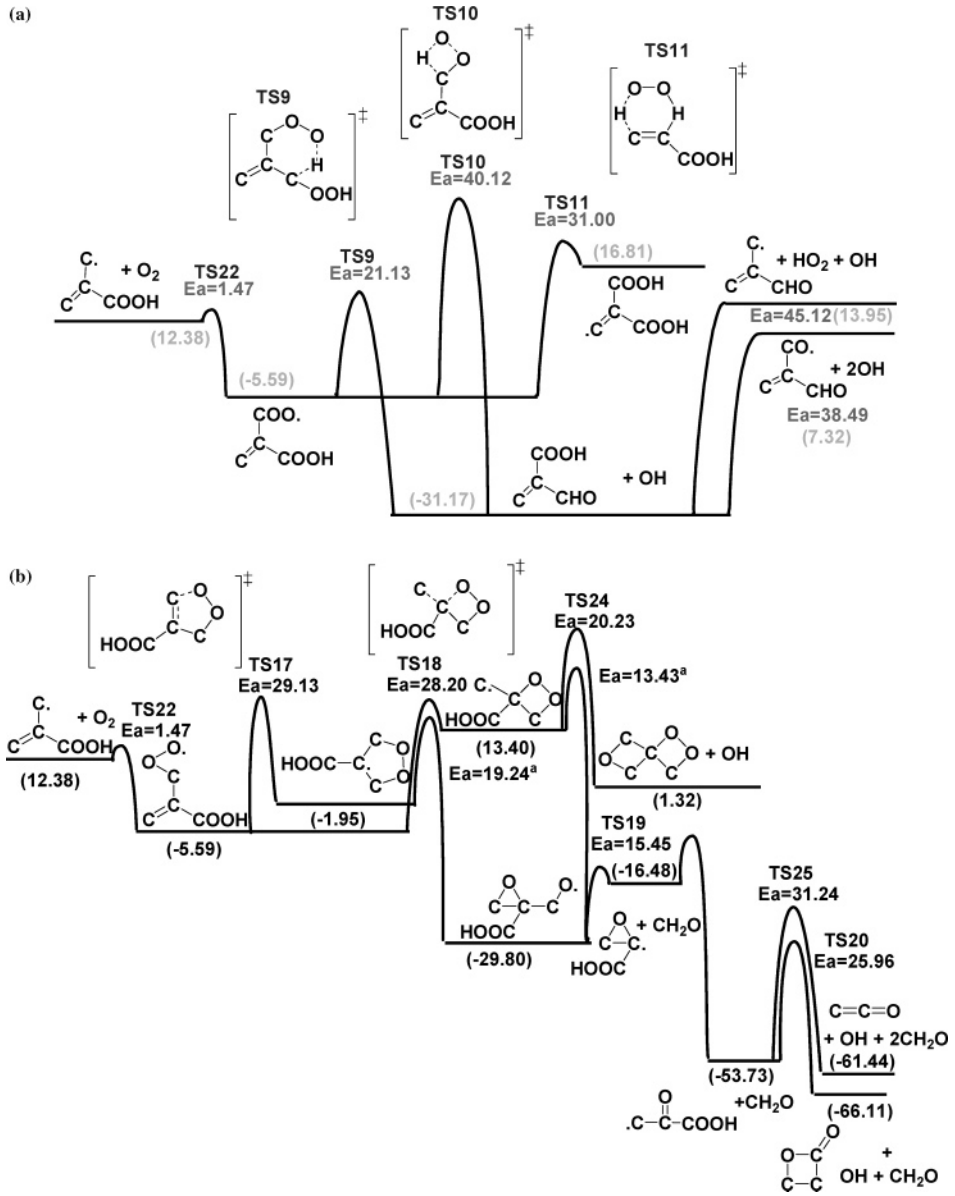

Figure 2. Potential energy diagrams for the C═C(C•)COOH + O_2 reaction system: (a) isomerization pathways; (b) cyclization pathways. (Units in kcal/mol.)

[a] The E_a value is taken as that of the first O_2 addition.

The well depth for C═C(C•)COOH + O_2 → C═C(COO•)-COOH is 17.97 kcal/mol, which is 3 kcal/mol less than that of the first O_2 addition. This shallower well depth is caused not only by the loss of resonance stabilization but also by the additional interaction between the peroxy and hydroperoxy groups in C═C(COO•)COOH, which results in higher energy. Reaction channels for the chemically activated adduct C═C(COO•)COOH* include dissociation back to reactants, stabilization to C═C(COO•)COOH, isomerizations through intramolecular H shift (Figure 2a), and cyclizations to form cyclic adducts (Figure 2b).

For the isomerization reactions of C═C(COO•)COOH, there are three different reaction pathways via transition states of TS9, TS10, and TS11, respectively. The reaction channels of both TS9 (E_a = 21.13 kcal/mol) and TS10 (E_a = 40.12 kcal/mol) produce OH + C═C(CHO)COOH. The forming C═C(CHO)-COOH has two dissociation channels: dissociating to HO_2 + C═C(C•)CHO with E_a = 45.12 kcal/mol and dissociating to OH + C═C(CO•)CHO with E_a = 38.49 kcal/mol. As shown in Figure S4a, the C═C(C•)CHO radical can undergo β-scission to form C═C═C + HCO via TS15 (E_a = 46.43 kcal/mol), and the C═C(CO•)CHO radical can dissociate to H + C═C(CHO)$_2$ through TS16 (E_a = 20.68 kcal/mol).

The isomer C•═C(COOH)$_2$ formed by the isomerization of C═C(COO•)COOH via TS11 (E_a = 31.00 kcal/mol), as shown in Figure S4b, can either react via TS12 (E_a = 20.42 kcal/mol) to form an OH radical and an oxetene product Cy(C═COC)-COOH, react via TS23 (E_a = 30.15 kcal/mol) to form C≡CCOOH, CH_2O, and OH, or directly dissociate to OH + C•═C(CO•)COOH. The H atom in the $-CH_2O$• group can dissociate from C•═C(CO•)COOH via TS13 (E_a = 24.97 kcal/mol) and generate C•═C(CHO)COOH, which dissociates to the OH radical and a four-membered-ring Cy(C═COC)CHO product. At higher temperatures, the stable product Cy(C═COC)COOH can undergo dissociation to form OH and Cy(C═COC)CO• (E_a = 39.40 kcal/mol), which further loses one H radical and forms Cy(C═COC)CHO via TS21 (E_a = 22.49 kcal/mol).

Aside from the above isomerization and subsequent reactions, the chemically activated adduct C═C(COO•)COOH* can also undergo cyclization pathways as shown in Figure 2b. The

TABLE 4: Comparison and Estimation of the Activation Energies (kcal/mol) for Similar Channels

	B3LYP	CBS-QB3	ΔE_a		B3LYP	corrected
TS2	38.62	36.48	−2.15	TS10	40.12	37.98
TS3	21.96	20.91	−1.05	TS9	21.13	20.08
TS4	13.55	14.50	0.95	TS19	15.45	16.41
TS6	30.09	26.83	−3.26	TS18	28.20	24.94
TS7	27.51	25.45	−2.06	TS17	29.13	27.08

terminal peroxy oxygen radical can interact with either side of the C═C π bond forming four (TS18, E_a = 28.20 kcal/mol) and five (TS17, E_a = 29.13 kcal/mol) -membered cyclic peroxides. The carbon radicals in both cyclic peroxides can interact with one of the peroxy oxygen atoms in the ring to form a three-membered-ring radical CO•Cy(COC)COOH, which undergoes β-scission through TS19 (E_a = 15.45 kcal/mol) to formaldehyde and the Cy(CO•C)COOH radical, which will quickly isomerize to the C•C(═O)COOH radical. The C•C(═O)COOH radical can further dissociate to two product sets: OH and O═CyCCOC via TS20 (E_a = 25.96 kcal/mol); and CH_2═C═O, CH_2O, and OH via TS25 (E_a = 31.24 kcal/mol). The carbon radical in the four-membered-ring cyclic peroxide C•-Cy(COOC)COOH can also interact with one peroxy oxygen in the −COOH group to form a product with two rings and OH via TS24 with a barrier of 20.23 kcal/mol.

Table 3b lists the total energy differences between TSs and reactants, intermediates, and products for reactions involved in the second O_2 addition at the DFT level. The dominant reaction pathway for the adduct C═C(COO•)COOH* is to dissociate back to reactants and isomerize to OH + C═C(CHO)COOH. Although the cyclization reactions have higher energy barriers, the energies for the product channels are much lower than that of the entrance channel. In addition, the concentrations of the cyclic peroxides are actually controlled by temperature, pressure, and concentrations of initial reactants and other radicals. As a result, the cyclization reactions are important pathways for heat release in the isobutenyl + O_2 system. Overall, the second O_2 addition also exhibits low reactivity toward oxygen because of the shallow well depth and high energy barriers for the subsequent isomerization and cyclization reactions. Together with the first O_2 addition, the above kinetic analyses quantitatively explain the antiknock behavior of isobutene.

Activation Energy Correction. Because of the similarities between the C═C(C)COO• and C═C(COO•)COOH geometries, the first and second O_2 addition systems have some similar reaction channels. For instance, both TS2 and TS10 have the structures of the peroxy oxygen attacking the H atom in the nearest secondary methyl group, and consequently, they have very close activation energies, i.e., 38.62 kcal/mol for TS2 and 40.12 kcal/mol for TS10. As a consequence of this similarity, the differences in the activation energies between the DFT and CBS-QB3 levels for reactions in the first O_2 addition could be used to correct the activation energies of similar reactions in the second O_2 addition for improved accuracy. For instance, the activation energy of TS2 at the CBS-QB3 level is 2.15 kcal/mol lower than that at the DFT level. Since TS2 and TS10 are the transition states for similar channels, the same energy difference between the DFT and CBS-QB3 levels from TS2 can be applied to TS10, which leads to a corrected activation energy of 40.12 − 2.15 = 37.98 kcal/mol for TS10. In the same manner, the activation energies were corrected for a number of reactions in the second O_2 addition system, as listed in Table 4. These corrected activation energies were used in the calculation of the enthalpies of formation for the corresponding transition states.

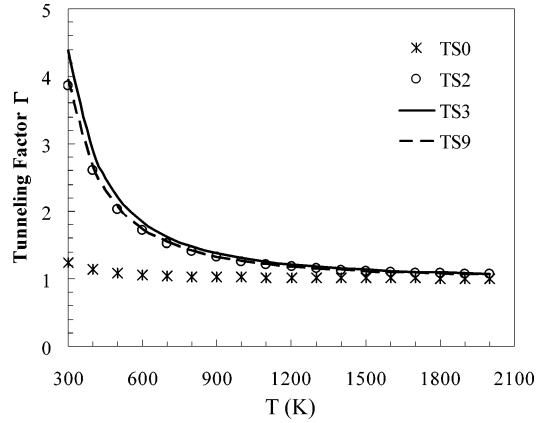

Figure 3. Calculated tunneling factors as functions of temperature for reaction pathways of TS0, TS2, TS3, and TS9.

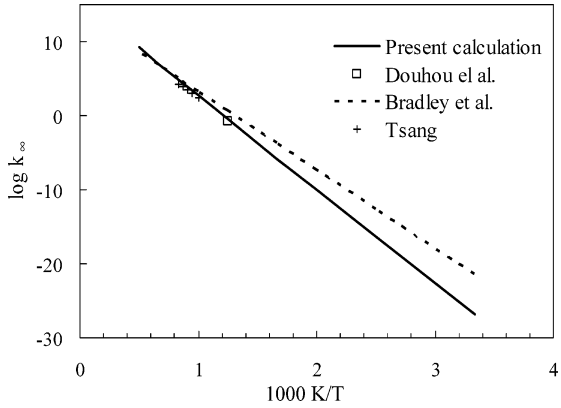

Figure 4. Comparison of the calculated high-pressure limit rate constants of C═C(C•)C → C═C═C + CH_3 with literature data.

3.5. High-Pressure Limit Rate Constants. On the basis of the conventional transition state theory, the calculated enthalpies and entropies for the species on the potential energy diagrams were employed to calculate the Arrhenius preexponential factors and the activation energies as functions of temperature for unimolecular isomerization and dissociation reactions. A couple of reactions involve the H-atom transfer process, including TS2, TS3, and TS9, and so, the tunneling effect on these reaction rates was taken into account using the following Wigner's equation:[34]

$$\Gamma = 1 + \frac{1}{24}\left(\frac{h\nu}{k_B T}\right)^2\left(1 + \frac{k_B T}{E_c}\right)$$

where Γ is the tunneling factor, h the Planck constant, k_B the Boltzmann constant, ν the imaginary asymmetric stretching frequency of the transition state, and E_c the activation energy without zero-point energy corrections. The calculated tunneling factors are plotted as functions of temperature in Figure 4 for TS2, TS3, and TS9. As expected, the tunneling effect is prominent mainly at low to moderate temperature and tends to diminish at high temperature. These tunneling factors were further used to correct the high-pressure limit rate constants (k_∞), which were subsequently fitted by three parameters, A, n, and E_a, over a temperature range 300−2000 K, as expressed by $k_\infty = AT^n \exp(-E_a/RT)$, by the *THERMKIN*[22] program. The fitted A, n, and E_a are listed in Table 5. They can be further used for QRRK or RRKM calculation for the pressure-dependent rate constants.

Few direct experimental measurements are available to validate our calculated elementary reaction rates in the isobute-

TABLE 5: High-Pressure Limit Rate Constants

reaction	A (s^{-1} or $cm^3/mol-s$)	n	E_a (kcal/mol)
C=C(C•)C → TS0 → C=C=C + CH_3•	7.10×10^{10}	1.38	56.36
C=C(C)COO• → TS2 → C=C(C)C=O + OH[a]	8.01×10^{5}	1.86	34.77
C=C(C)COO• → TS3 → C=C(C•)COOH[a]	4.87×10^{3}	2.13	18.76
CCy(CCO)CO• → TS4 → CCy(C•CO) + CH_2O	1.63×10^{12}	0.57	14.83
C=C(C•)COOH → TS5 → C=CyCCOC + OH	1.13×10^{10}	0.56	33.11
C=C(C)COO• → TS6 → C_2•CyCOOC	2.45×10^{6}	1.47	26.36
C=C(C)COO• → TS7 → CCyC•COOC	9.28×10^{7}	0.88	25.17
C_2•CyCOOC → TS8 → CCy(CCO)CO•	2.39×10^{11}	0.34	13.79
C=C(COO•)COOH → TS9 → C=C(CHO)COOH + OH[a]	6.61×10^{5}	1.37	18.19
C=C(COO•)COOH → TS10 → C=C(CHO)COOH + OH	4.97×10^{6}	1.54	37.24
C=C(COO•)COOH → TS11 → C•=C$(COOH)_2$	2.03×10^{8}	1.20	30.82
C•=C$(COOH)_2$ → TS12 → Cy(C=COC)COOH + OH	2.74×10^{5}	1.92	19.13
C•=C(CO•)COOH → TS13 → C•=C(CHO)COOH + H	5.13×10^{8}	1.46	24.60
C•=C(CHO)COOH → TS14 → Cy(C=COC)CHO + OH	4.46×10^{6}	1.53	17.84
C=C(C•)CHO → TS15 → C=C=C + HCO	2.92×10^{12}	0.84	46.72
C=C(CO•)CHO → TS16 → C=C$(CHO)_2$ + H	4.14×10^{10}	1.02	20.85
C=C(COO•)COOH → TS17 → Cy(C•COOC)COOH	2.62×10^{12}	-0.21	27.40
C=C(COO•)COOH → TS18 → C•Cy(COOC)COOH	4.24×10^{9}	0.66	24.91
CO•Cy(COC)COOH → TS19 → Cy(C•OC)COOH + CH_2O	1.29×10^{13}	0.43	15.84
C•C(=O)COOH → TS20 → O=CyCCOC + OH	4.64×10^{13}	-0.32	26.42
Cy(C=COC)CO• → TS21 → Cy(C=COC)CHO + H	1.39×10^{10}	0.90	22.53

[a] Tunneling effect was included.

nyl radical oxidation system. Nonetheless, for the isobutenyl radical dissociation reaction C=C(C•)C → TS0 → C=C=C + CH_3, there are a few published high-pressure limit rate constants. Tsang[35] studied the 2,4-dimethylhexene-1 decomposition in single-pulse shock tube experiments. By fitting the experimental data to a complex mechanism of 2,4-dimethylhexene-1 dissociation, the reaction constant for the isobutenyl radical dissociation to allene plus methyl radical was derived at the beginning of the falloff regime over the temperature range 968−1180 K, and the high-pressure limit rate constant was further derived on the basis of the RRK calculation. Bradley and West[36] estimated this high-pressure rate constant by considering the entropy changes involved in the transition state for the preexponential A factor, with the activation energy being derived from overall thermochemistry. Douhou et al.[37] calculated the high-pressure-limit rate constant on the basis of equilibrium conditions at 800 K and the reverse rate constant of Tsang.[34] The high-pressure rate coefficients by Tsang,[34] Bradley and West,[36] and Douhou et al.[37] are

$$k_\infty = 10^{13.58} \exp(-50\,872/RT)\ \mathrm{sec}^{-1} \qquad \text{(Tsang)}$$

$$k_\infty = 10^{14} \exp(-48\,517/RT)\ \mathrm{sec}^{-1} \qquad \text{(Bradley and West)}$$

$$k_\infty = 10^{13.9} \exp(-53\,600/RT)\ \mathrm{sec}^{-1} \qquad \text{(Douhou et al.)}$$

The high-pressure rate constant determined in the present study is

$$k_\infty = 7.10 \times 10^{10} \times T^{1.38} \exp(-56\,356/RT)\ \mathrm{sec}^{-1}$$

as shown in Table 5. Figure 4 shows the comparison of the above high-pressure limit rate constants of the isobutenyl radical dissociation reaction. It is seen that our data agree well with those of Douhou et al. and Tsang at their validated temperature ranges and overall are more accurate than those estimated by Bradley et al. We recommend our high-pressure rate constants because they were calculated from high-level ab initio theory by implementing the canonical transition state theory and were fitted over a broad temperature range 300−2000 K. Since the same methodology for the calculation of high-pressure limit rate constants was used for all unimolecular reactions in this study, our other recommended high-pressure limit rate constants should have similar accuracy.

There are two more remarks on reaction C=C(C•)C → TS0 → C=C=C + CH_3. First, the influence of tunneling estimated by the Wigner's equation[34] is negligible, as shown in Figure 3, so it is not included in Table 5. Second, according to Brezinsky and Dryer,[6] this reaction is responsible for the antiknock behavior of isobutene. The isobutenyl radical is formed from the H-abstraction reaction of isobutene by reactive OH and H radicals and then dissociates to two nonreactive allene and methyl radicals. As a result, these two reactions serve as a radical sink and consequently slow the ignition process. Our new result on this reaction rate constant will be helpful in improving the quantification of isobutene's inhibitive effect on ignition.

4. Summary

The thermochemical properties of reactants, important intermediates, transition states, and products in the isobutenyl radical + O_2 reaction system and the 2-hydroperoxymethyl-2-propenyl radical + O_2 reaction system were calculated by using ab initio CBS-QB3, G3(MP2), and density functional B3LYP/6-311G-(d,p) methods. The reaction kinetics of the second O_2 addition to the isobutenyl radical was analyzed by using density functional theory. Since the first and second O_2 addition systems have some similar reaction pathways, we calculated several important reactions in the first O_2 addition system at the higher CBS-QB3 and G3(MP2) levels and corrected the activation energies of similar reactions in the second O_2 addition by the energy differences between the high-level ab initio and DFT calculation for improved accuracy. Then, the high-pressure rate constants for important unimolecular reactions were determined as functions of temperature by the canonical transition state theory for further kinetic model development.

The kinetic analysis revealed that, because of the resonance stabilization of the isobutenyl radical, the addition reactions with O_2 have shallow well depths, and only certain isomerization reactions (TS3, TS9) have comparable energy barriers. Consequently, the major reaction pathways for the formed adduct in both O_2 addition systems are dissociation back to the reactants and isomerization through H-atom transfer. Overall, addition of O_2 to the isobutenyl radical has low reactivity at low

temperature, which is responsible for the antiknock behavior of isobutene.

Acknowledgment. This research was supported by the Army Research Office under the technical monitoring of Dr. David Mann.

Supporting Information Available: Optimized structural parameters of 50 species, including transition state structures (Table S-1), the corresponding unscaled vibrational frequencies, and moments of inertia (Table S-2). Names for some important species (Table S-3). Illustration of contributions of TVR and IR to entropies and heat capacities (Table S-4). The torsional potentials on the C—C, C—O, and O—O bonds calculated at the B3LYP/6-311G(d,p) level (Figures S1−S3). Reaction pathway analyses of the intermediates in the C═C(C•)COOH + O_2 reaction system (Figure S4). This material is available free of charge via the Internet at http://pubs.acs.org.

References and Notes

(1) Dryer, F. L.; Brezinsky K. *Combust. Sci. Technol.* **1986**, *45* (3−4), 199.
(2) Surygala, J.; Sliwka, E. *Przem. Chem.* **2002**, *81* (2), 115.
(3) Dutz, M.; Krahl, J.; Bunger, J. *Landbauforsch. Volkenrode* **2002**, *52* (3), 175.
(4) Elkadi, B.; Baronnet, F. *J. Chim. Phys. Phys. Chim. Biol.* **1995**, *92* (3), 706.
(5) Brocard, J. C.; Baronnet, F.; O'Neal H. E. *Combust. Flame* **1983**, *52* (1), 25.
(6) Brezinsky K.; Dryer, F. L. *Combust. Sci. Technol.* **1986**, *45* (5−6), 225.
(7) Bauge, J. C.; Battin-Leclerc, F.; Baronnet, F. *Int. J. Chem. Kinet.* **1998**, *30*, 629.
(8) Dagaut, P.; Cathonnet, M. *Combust. Sci. Technol.* **1998**, *137*, 237.
(9) Curran, H. J.; Dunphy, M. P.; Simmie, J. M.; Westbrook, C. K.; Pitz, W. J. *Proc. Combust. Inst.* **1992**, *24*, 769.
(10) Curran, H. J. Ph.D. Thesis, National University of Ireland, Galway, 1994.
(11) Ingham, T.; Walker, R. W.; Woolford, R. E. *Proc. Combust. Inst.* **1994**, *25*, 767.
(12) Chen, C. J.; Bozzelli, J. W. *J. Phys. Chem. A* **2000**, *104*, 9715.
(13) Minetti R.; Roubaud A.; Therssen E.; Ribaucour M.; Sochet L. R. *Combust. Flame* **1999**, *118* (1−2), 213.
(14) Montgomery, J. A.; Frisch, M. J.; Ochterski, J. W.; Petersson, G. A. *J. Chem. Phys.* **1999**, *110*, 2822.
(15) Curtiss, L. A.; Redfern, P. C.; Raghavachari, K.; Rassolov, V.; Pople, J. A. *J. Chem. Phys.* **1999**, *110*, 4703.
(16) Curtiss, L. A.; Raghavachari, K.; Redfern, P. C.; Rassolov, V.; Pople, J. A. *J. Chem. Phys.* **1998**, *109*, 7764.
(17) Curtiss, L. A.; Raghavachari, K.; Pople, J. A. *J. Chem. Phys.* **1993**, *98*, 1293.
(18) Frisch, M. J.; Trucks, G. W.; Schlegel, H. B.; Scuseria, G. E.; Robb, M. A.; Cheeseman, J. R.; Montgomery, J. A., Jr.; Vreven, T.; Kudin, K. N.; Burant, J. C.; Millam, J. M.; Iyengar, S. S.; Tomasi, J.; Barone, V.; Mennucci, B.; Cossi, M.; Scalmani, G.; Rega, N.; Petersson, G. A.; Nakatsuji, H.; Hada, M.; Ehara, M.; Toyota, K.; Fukuda, R.; Hasegawa, J.; Ishida, M.; Nakajima, T.; Honda, Y.; Kitao, O.; Nakai, H.; Klene, M.; Li, X.; Knox, J. E.; Hratchian, H. P.; Cross, J. B.; Bakken, V.; Adamo, C.; Jaramillo, J.; Gomperts, R.; Stratmann, R. E.; Yazyev, O.; Austin, A. J.; Cammi, R.; Pomelli, C.; Ochterski, J. W.; Ayala, P. Y.; Morokuma, K.; Voth, G. A.; Salvador, P.; Dannenberg, J. J.; Zakrzewski, V. G.; Dapprich, S.; Daniels, A. D.; Strain, M. C.; Farkas, O.; Malick, D. K.; Rabuck, A. D.; Raghavachari, K.; Foresman, J. B.; Ortiz, J. V.; Cui, Q.; Baboul, A. G.; Clifford, S.; Cioslowski, J.; Stefanov, B. B.; Liu, G.; Liashenko, A.; Piskorz, P.; Komaromi, I.; Martin, R. L.; Fox, D. J.; Keith, T.; Al-Laham, M. A.; Peng, C. Y.; Nanayakkara, A.; Challacombe, M.; Gill, P. M. W.; Johnson, B.; Chen, W.; Wong, M. W.; Gonzalez, C.; Pople, J. A. *Gaussian 03*, revision B.04; Gaussian, Inc.: Pittsburgh, PA, 2003.
(19) Sun, H.; Bozzelli, J. W. *J. Phys. Chem. A* **2004**, *108* (10), 1694.
(20) Sun, H.; Chen, C. J.; Bozzelli, J. W. *J. Phys. Chem. A* **2000**, *104*, 8270.
(21) Sun, H.; Bozzelli, J. W. *J. Phys. Chem. A* **2003**, *107*, 1018.
(22) Sheng, C. Ph.D. Thesis, New Jersey Institute of Technology, Newark, NJ, 2002.
(23) Blanksby, S. J.; Ramond, T. M.; Davico, G. E.; Nimlos, M. R.; Kato, S.; Bierbaum, V. M.; Lineberger, W. C.; Ellison, G. B.; Okumura, M. *J. Am. Chem. Soc.* **2001**, *123* (39), 9585.
(24) Chen, C.-J.; Bozzelli, J. W. *J. Phys. Chem. A* **2000**, *104*, 4997.
(25) Knyazev, V. D.; Slage, I. R. *J. Phys. Chem. A* **1998**, *102*, 1770.
(26) Rodgers, A. S. *Selected Values for Properties of Chemical Compounds*; Thermodynamic Research Center (TRC), Texas A&M University: College Station, TX, 1982.
(27) Ritter, E. R.; Bozzelli, J. W. *Int. J. Chem. Kinet.* **1991**, *23*, 767.
(28) Cox, J. D.; Pilcher, G. *Thermochemistry of Organic & Organometallic Compounds*; Academic Press: London, 1970.
(29) Jenkin, M. E.; Murrells, T. P.; Shalliker, S. J.; Hayman, G. D. *J. Chem. Soc., Faraday Trans.* **1993**, *89*, 433.
(30) Slagle, I. R.; Park, J.-Y.; Heaven, M. C.; Gutman, D. *J. Am. Chem. Soc.* **1984**, *106*, 4356.
(31) Ruiz, R. P.; Bayes, K. D.; Macpherson, M. T.; Pilling, M. J. *J. Phys. Chem.* **1981**, *85*, 1622.
(32) We were not able to locate the structure of TS5 at the HF/6-31G-(d,p) level, so the zero-point energy and the thermal correction were instead taken at the MP2 level for the G3(MP2) calculation.
(33) We were not able to locate the structure of TS8 at the MP2(full)/6-31G(d) and HF/6-31G(d,p) levels, so the geometry, the zero-point energy, and the thermal correction were instead taken at the B3LYP/6-311G(d,p) level for the G3(MP2) calculation.
(34) Shavitt, I. *J. Chem. Phys.* **1959**, *31*, 1359.
(35) Tsang, W. *Int. J. Chem. Kinet.* **1973**, *5*, 929.
(36) Bradley, J. N.; West, K. O. *J. Chem. Soc., Faraday Trans. 1* **1976**, *72*, 8.
(37) Douhou, S.; Perrin, D.; Martin, R. *J. Chim. Phys.* **1994**, *91*, 1597.